ELSEVIER

Tectonophysics 279 (1997) 281–302

TECTONOPHYSICS

Fluid circulation related to deformation in the Zabargad gneisses (Red Sea rift)

Anne-Marie Boullier [a,*], Karima Firdaous [b], Françoise Boudier [c]

[a] *Laboratoire de Géophysique Interne et Tectonophysique, C.N.R.S., B.P. 53X, F-38041 Grenoble Cedex, France*
[b] *Centre de Recherches Pétrographiques et Géochimiques, C.N.R.S., B.P. 20, F-54501 Vandoeuvre-lès-Nancy Cedex, France*
[c] *Laboratoire de Tectonophysique, C.N.R.S., Université de Montpellier 2, Place E. Bataillon, F-34095 Montpellier Cedex, France*

Accepted 2 May 1997

Abstract

A fluid inclusion study in relation to textures has been performed on Pan-African granulite-facies gneisses from Zabargad Island (Red Sea rift, Egypt). The gneiss samples were collected at a maximum distance of 60 m above the contact with mantle peridotites with which they are co-structured by a high-T plastic deformation during an isothermal decompression starting from conditions estimated at 35 km depth and 850°C (base of the Pan-African crust). A first metasomatism of the crustal section during decompression is represented by CO_2-fluid inclusions trapped at minimum conditions of 15 km depth and 800°C. The CO_2-fluid inclusion planes are controlled in orientation by the high-T plastic flow structures, but have been subsequently deformed during medium-T plastic deformation in quartz. The second metasomatism is represented by solid-rich aqueous fluid inclusions which were trapped at minimum P–T conditions of 3.7 km depth and 450°C corresponding to a very high thermal gradient. They trace the introduction either of seawater or of fluids resulting from leaching of the Middle Miocene evaporites, within the gneisses during their residence at a shallow depth below the seafloor. Two models are proposed in the literature in order to reconstruct the geodynamic history of Zabargad Island: one [Brueckner, H.K., Elhaddad, M.A., Hamelin, B., Hemming, S., Kröner, A., Reisberg, L., Seyler, M., 1995, A Pan African origin and uplift for the gneisses and peridotites of Zabargad Island, Red Sea: a Nd, Sr, Pb and Os isotope study, J. Geophys. Res. 100, 22283–22297] suggests that most of the decompression P–T path is Pan-African in age and only the aqueous metasomatism is related to the rifting history of the Red Sea; the second [Nicolas, A., Boudier, F., Montigny, R., 1987, Structure of Zabargad Island and early rifting of the Red Sea, J. Geophys. Res. 92, 461–474; Boudier, F., Nicolas, A., Ji, S., Kienast, J.R., Mevel, C., 1988, The gneiss of Zabargad Island: deep crust of a rift, Tectonophysics 150, 209–227] supposes the existence of an asthenospheric diapir intrusive through the deep Pan-African crust leading to a continuous deformation event during early rifting of the Red Sea. Although it is impossible to date trapping of fluid inclusions and to know with certainty the origin of the fluids, our preference is for the second model but slightly modified. The high-T decompression path traced by CO_2-fluid inclusions, relayed by solid-rich aqueous inclusions, traces a continuous process of crustal thinning. Such a continuous path would assign to a single event the thinning and uplift of the deep crust and uppermost lithosphere to shallow basin bottom during the Red Sea early rifting. In such an interpretative model, the northern and central peridotite bodies are representative of the uppermost continental lithosphere and only the southern body could belong to an ascending asthenospheric diapir centred on the southeast of Zabargad Island.

Keywords: Zabargad; Red Sea rift; gneisses; fluid inclusions

* Corresponding author. Fax: +33-4-76-82-81-01; e-mail: Anne-Marie.Boullier@obs.ujf-grenoble.fr

PII S0040-1951(97)00116-9

1. Introduction

Zabargad Island is situated on the western margin of the Red Sea main trough (Fig. 1). In spite of its small size (4 km^2), it has been the subject of numerous recent geological, geophysical, petrographical and geochemical studies due to the presence of mantle rock outcrops in a rifting geological setting. The peridotites are associated with a metamorphic gneiss complex. Two contradictory interpretations were suggested for the origin of these gneisses: old Pan-African (ca. 600 Ma) continental crust (El Ramly, 1972), or new crust formed by the metamorphism of rift sediments and mafic intrusions (Nicolas et al., 1987). The first interpretation was confirmed by geochronological studies (Lancelot and Bosch, 1991; Brueckner et al., 1995) showing that all the granulite-facies felsic gneisses are remnants of a Pan-African continental crust. However, Bonatti and Seyler (1987) and Boudier et al. (1988), on the basis of petrological and structural data, concluded to a mixed origin: new intrusive mafic components were added to remnants of Pan-African continental crust.

The controversy now concerns the age of the juxtaposition of the granulites and peridotites, and the lithospheric or asthenospheric nature of the latter (Brueckner et al., 1995). The gneisses of Zabargad Island are in contact with lherzolites that were interpreted either as a mantle diapir emplaced during the early rifting of the Red Sea (Bonatti et al., 1981; Nicolas et al., 1987) or as mantle material emplaced into the crust during Pan-African convergence (Brueckner et al., 1995). The gneisses were metamorphosed and deformed in the granulite to amphibolite facies (Seyler and Bonatti, 1988; Boudier et al., 1988) along with the peridotite as shown by the common kinematics registered by the two rock types. This paper is focussed on the relationships between textures of the gneisses and gabbros, and the fluid inclusions representative of the fluid circulation in order to bring some new information on fluid circulation in the crustal sequence of Zabargad Island and, if possible, to distinguish the respective contributions of metamorphic or mantle fluids and of seawater during the deformation events.

2. Geological context

The main geological units of Zabargad Island are the following (Fig. 1).

(1) Plagioclase peridotites (southern body) and spinel lherzolites (central and northern bodies), which are proposed to have a mantle controversial origin in relation with the Red Sea opening (Bonatti et al., 1981; Styles and Gerdes, 1983; Nicolas et al., 1985).

(2) Granulite-facies gneisses, which occupy the western and the central part of the island and have been dated as part of the Pan-African basement (Lancelot and Bosch, 1991; Brueckner et al., 1995).

(3) The Zabargad Formation, which is a sedimentary formation made of an alternation of black shales and grits and tectonically overlies the gneisses and peridotites. It is affected by a low-grade metamorphism which has been related to the contact metamorphism of diabase sills intruded at the base of this formation (Nicolas et al., 1985).

(4) Numerous diabase dykes, which cross-cut both the peridotite and gneiss formations and diabase sills which are well developed in the contact between the peridotite and the Zabargad Formation.

(5) The evaporite unit of Middle Miocene age (Bonatti et al., 1983), which discordantly overlies the Zabargad Formation and is not metamorphic.

(6) Older and recent reef carbonates.

Both the gneiss complex and the peridotites have a complicated structural and metamorphic history at high pressure and temperature (Nicolas et al., 1987; Boudier et al., 1988). Most models proposed that this history occurred during the opening of the Red Sea as a mantle diapir intruded into the crust (Bonatti et al., 1981; Styles and Gerdes, 1983; Nicolas et al., 1985).

3. Description of the gneisses

Petrography, mineralogy and geochemistry of the gneisses have already been described by Bonatti and Seyler (1987), Seyler and Bonatti (1988) and Boudier et al. (1988). Only the major features are given here. The different components of the gneisses are: (1) granulites s.str. which have tonalitic–trondhjemitic affinities (Bonatti and Seyler, 1987); (2) deformed meta-gabbros and pyroxenites recrystallized into mafic granulites or amphibolites and which are rem-

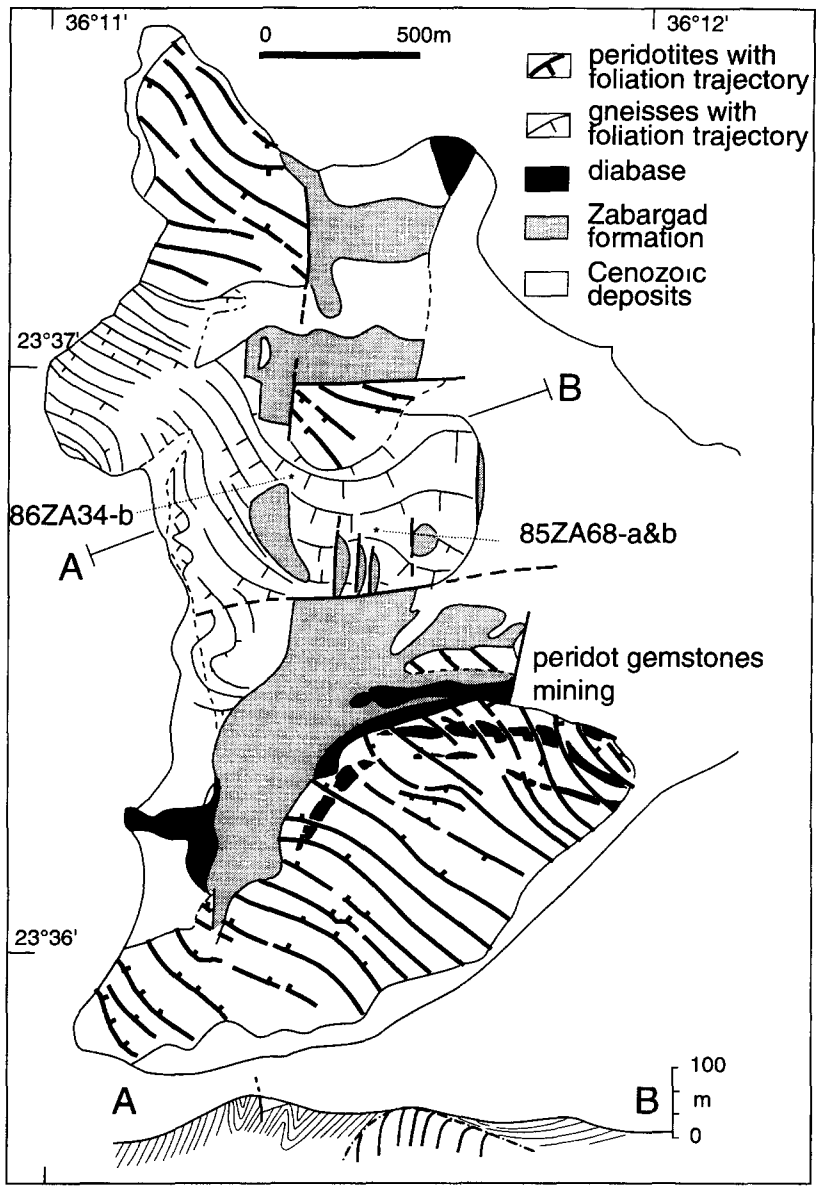

Fig. 1. Schematic map and cross-section A–B of Zabargad Island (modified from Boudier et al., 1988). Location of the studied samples.

nants of a basic layered complex; and (3) basaltic dykes which cross-cut the peridotites and gneisses (Bonatti and Seyler, 1987; Seyler and Bonatti, 1988). Boudier et al. (1988) distinguish two sets of diabase dykes which are not or only slightly deformed in the peridotites but which are discordant to concordant relative to the foliation of the gneisses when approaching the contact with the peridotites along a strain gradient and which are transformed into foliated amphibolites. Moreover, the occurrence at the same place of discordant and subconcordant dykes suggests that these diabase dykes were intruded continuously during the deformation of the enclosing rocks.

This study focuses on two samples of the granulites s.str. (85ZA68-a and 85ZA68-b) and one sample of metagabbro (86ZA34b) from the point of

view of relationships between textures and fluid inclusions. The petrography and mineralogy of these three samples have been described by Boudier et al. (1988). One of these samples (85ZA68-b) has been studied by Lancelot and Bosch (1991) for geochronology. They were collected in two outcrops (Fig. 1) at a maximum distance of 60 m (normal to the foliation) above the contact with mantle peridotites with which they are co-structured. Only one foliation (115 S 15) and one lineation (subhorizontal E–W) are discernable on both outcrops (no superimposed schistosity or folding phase) although an earlier foliation could have been preserved in some other places (Marshak et al., 1992). A three-phase metamorphic history may be recognized from the successive mineral assemblages in these samples and confirms the previous observations made by Bonatti and Seyler (1987), Seyler and Bonatti (1988) and Boudier et al. (1988).

3.1. Sample 85ZA68-b

This sample shows a foliation defined by flattened garnets, pyroxenes and stretched aggregates of plagioclase and quartz and a lineation defined by the same constituents. A first granulite-facies assemblage (stage I) is made of plagioclase I + garnet + orthopyroxene + clinopyroxene + quartz. It is replaced by a second assemblage (stage II) defined by a corona of polygonal plagioclase II (andesine–oligoclase), already described by Bonatti and Seyler (1987) in similar rocks, and by a rim of colourless amphibole, biotite and magnetite–ilmenite. The latter are observed also in the grain boundaries between the polygonal plagioclases II around the flattened garnet (Fig. 2). These amphibole, biotite and magnetite–ilmenite minerals are themselves interpreted as the product of hydration of the previous orthopyroxene resulting from the transformation:

garnet + quartz = plagioclase II + orthopyroxene

Garnet was partly kelyphytized along margins and fractures (vermicules of biotite, plagioclase, magnetite–ilmenite) during this metamorphic hydration stage. Furthermore, colourless or pale amphiboles are surrounded by a rim of green to blue-green amphibole which is characterized by a high chlorine content (Boudier et al., 1988).

The main foliation of the sample is defined by the minerals of both the first and the second assemblages, i.e. pyroxenes, garnet, plagioclase I and II and quartz. The quartz ribbons have also registered a slight plastic deformation as shown by dynamic recrystallization into small grains (50 μm) along

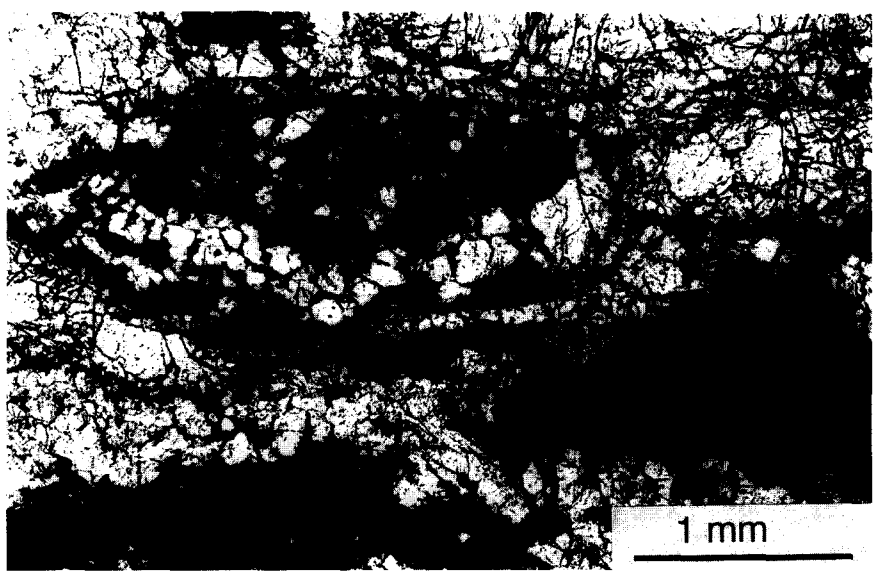

Fig. 2. Microphotograph of the 85ZA68-b sample showing garnet relicts surrounded by a plagioclase and ferro-magnesian mineral assemblage. Plane polarized light. Trace of the foliation plane and stretching lineation are parallel to the length of the microphotograph.

the grain boundaries and undulatory extinction with prismatic tight subgrains. The products of hydration of granulites have no preferred orientation and developed statically upon the previous structures.

Fluid inclusions are present within garnet, plagioclase I and II, quartz, pyroxenes where not replaced by amphiboles, within accessory minerals such as apatite and zircon and along quartz grain boundaries.

3.2. Sample 85ZA68-a

This sample corresponds to a more felsic constituent of the gneisses. It is made of quartz, entirely kelyphytized garnet, plagioclase and amphibolitized clinopyroxene. Therefore, the three metamorphic stages are not so clearly expressed in this sample. However, textures are similar, that is flattening and stretching of minerals from granulite-facies metamorphic stages and plastic deformation and dynamic recrystallization of quartz ribbons before hydration (kelyphyte and amphiboles) of the third metamorphic stage.

Fluid inclusions are essentially present within quartz and plagioclase and along quartz grain boundaries. The complete transformation of other minerals (garnet and clinopyroxene) during the third metamorphic stage makes the recognition of fluid inclusions impossible.

3.3. Sample 86ZA34b

This is a foliated and lineated gabbro-norite which contains relict magmatic ortho- and clino-pyroxene, and plagioclase (stage I). The secondary assemblage formed during mylonitization and includes granular ortho- and clino-pyroxene, granular plagioclase and brown amphibole titanium-rich pargasite (stage II). Aluminium content is much lower in secondary than in primary pyroxenes, suggesting that the mylonitization took place at lower pressure than the crystallization of the gabbronorite (Boudier et al., 1988). The mylonitic deformation textures of this sample have been described by Ji et al. (1988) and ascribed to high-temperature deformation. Undeformed scapolites developed in cracks oriented at high angles to the foliation and lineation.

Fluid inclusions are present in all the mineral phases and along grain boundaries.

4. Fluid inclusion study

Fluid inclusions in minerals may be subdivided into two groups (see Roedder, 1984), i.e. the primary fluid inclusions which are contemporaneous with the mineral growth, and the secondary fluid inclusions which postdate the mineral growth. The secondary fluid inclusions are either within grain boundaries and result from redistribution of fluid inclusions during dynamic recrystallization (Hollister, 1990) or trapped in intracrystalline microfractures which are subsequently healed (see again Roedder, 1984). Therefore, secondary fluid inclusions within minerals are arranged in planar arrays which are called 'fluid inclusion planes' in this paper. In the samples studied, no primary fluid inclusion was found, and all the descriptions below concern secondary fluid inclusions which are present in almost all minerals as quoted above and along grain boundaries.

4.1. Analytical methods

Fluid inclusions have been investigated in thick (0.150 mm) oriented doubly polished sections. The 3D orientations of fluid inclusion planes were measured by using the calibrated focus screw of a standard petrographic microscope following the Ploegsma (1989) method.

Measurements of the phase transition temperatures in fluid inclusions (microthermometry) have been performed using a gas flow USGS-adapted Fluid. Inc. stage (see Roedder, 1984) calibrated with synthetic fluid inclusions supplied by Synflinc. P–V–T–X properties of the fluids are then deduced from the microthermometric data using state equations appropriate to fluid systems.

4.2. Different types of fluid inclusions

Based on petrographic observations on ca. 40 samples and microthermometric measurements (melting and homogenization temperatures), two main types of fluid inclusions have been observed in the Zabargad gneisses: CO_2-fluid inclusions and solid-rich aqueous fluid inclusions.

4.2.1. Type 1: CO_2-fluid inclusions

CO_2-fluid inclusions are present in all granulites, gabbros and metagabbros examined (total of 30 sam-

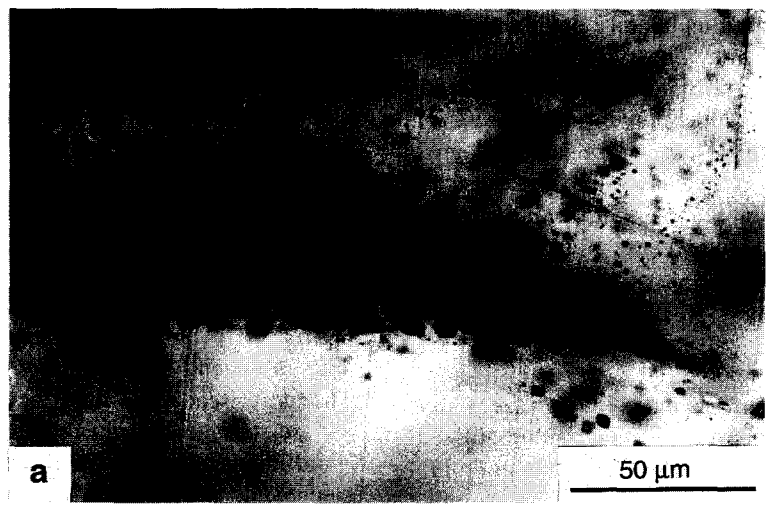
a
50 μm

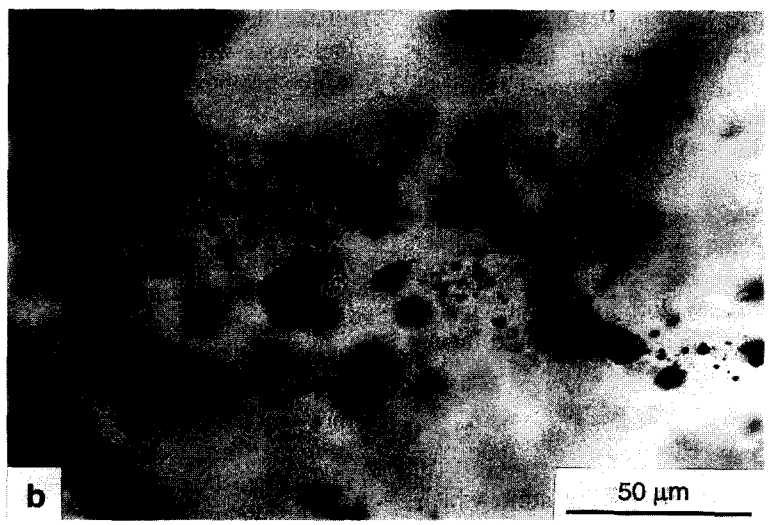
b
50 μm

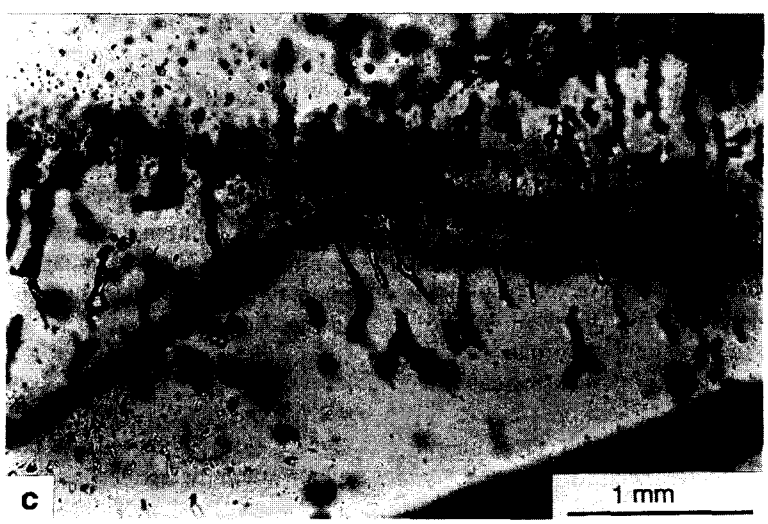
c
1 mm

ples) but were not observed in amphibolitized diabases (ca. 10 samples). Two subtypes have been distinguished.

Type 1a: liquid-rich CO_2-fluid inclusions. These are generally two-phased (liquid>vapour) at room temperature (20°C) or locally three-phased when they contain one, or more rarely two, small solids. They are secondary, i.e. within fluid inclusion planes or along grain boundaries.

In plagioclase or in pyroxene, they tend to have a rectangular shape parallel to the crystallographic planes of the host crystal (Fig. 3a); the largest CO_2-fluid inclusions (>4 μm) are spread out from the original microcrack leading to some uncertainty in the orientation measurement of these cracks. Garnet contains mostly very small two-phased CO_2-fluid inclusions.

In quartz, CO_2-fluid inclusions have variable shapes depending on their filling ratio (volume of the vapour bubble/total volume). In a single microcrack with low filling ratio, the smallest CO_2-fluid inclusions are regular, generally with a negative crystal shape, but the largest CO_2-fluid inclusions (>10 μm) are surrounded by a planar halo defined by very small CO_2-fluid inclusions which have a filling ratio identical to that of the large central one (Fig. 3b). Experimental results (Pêcher and Boullier, 1984; Boullier et al., 1989; Bodnar et al., 1989; Vityk and Bodnar, 1995) on similar features suggest that they can be interpreted as decrepitation halos originated from internal overpressure within the large fluid inclusions. Therefore, these fluid inclusions are called decrepitated type 1a CO_2-fluid inclusions.

There is a correlation between the size of fluid inclusions within a healed crack and the length of that crack: the shortest planes contain the smallest fluid inclusions. In the Zabargad samples, the healed cracks which contain small fluid inclusions are generally located in the vicinity of long planes containing large fluid inclusions.

Type 1b: vapour-rich CO_2-fluid inclusions. In quartz, some planes of large irregular CO_2-fluid inclusions are also observed in which fluid inclusions either have high filling ratios (large vapour bubble, Fig. 3c) or are one-phase fluid inclusions (vapour phase) at room temperature. These planes appear as incompletely healed fractures (unminimized surface energy). In one of those, it was possible to observe a water meniscus in thin tubes separating two large CO_2-fluid inclusions. In the 86ZA34-b gabbro, only type 1b irregular vapour-rich CO_2-fluid inclusions have been observed in the late undeformed scapolites.

4.2.2. Type 2: Solid-rich aqueous fluid inclusions

These fluid inclusions contain numerous solids with different shapes and a shrunk vapour bubble (Fig. 4a). Almost no liquid is visible at room temperature, but liquid appears during heating experiments when the solids disappear by dissolution. Their behaviour during heating experiments is comparable to that of the 'liquid-absent aqueous fluid inclusions' described by Schiffries (1990). The following solids were observed: a large cubic solid (halite), thin platelets and birefringent crystals, some of which show a relief pleochroism indicating that they may be carbonates or nahcolite. Observations were made on rock fragments with a S.E.M. in order to determine the nature of crystals in the open cavities (Fig. 4b). Semi-quantitative analysis on open fluid inclusions suggests the presence of $FeCl_2$, $CaCl_2$, dolomite, calcite, siderite and talc (?), minerals which accompany large halite crystals. Some phosphorus and sulphur (gypsum?) have also been detected in small solid phases. These solid-rich aqueous fluid inclusions are trapped in healed microcracks within all minerals.

In the 86ZA34-b gabbro, undeformed scapolites developed in cracks with the same orientation as the few observed solid-rich aqueous fluid inclusion planes.

4.3. Chronology of fluid inclusions

In general, the chronology of different types of fluid inclusions may be determined by cross-cutting relationships between healed microcracks (Touret,

Fig. 3. Plane polarized light microphotographs of carbonic fluid inclusions in the 85ZA68-b sample. (a) Rectangular-shape type 1a CO_2-fluid inclusions in plagioclase. (b) Large decrepitated type 1a CO_2-fluid inclusions surrounded by a halo of small secondary CO_2-fluid inclusions in quartz. (c) Large irregular-shape type 1b CO_2-fluid inclusions with a high filling ratio (large vapour bubble).

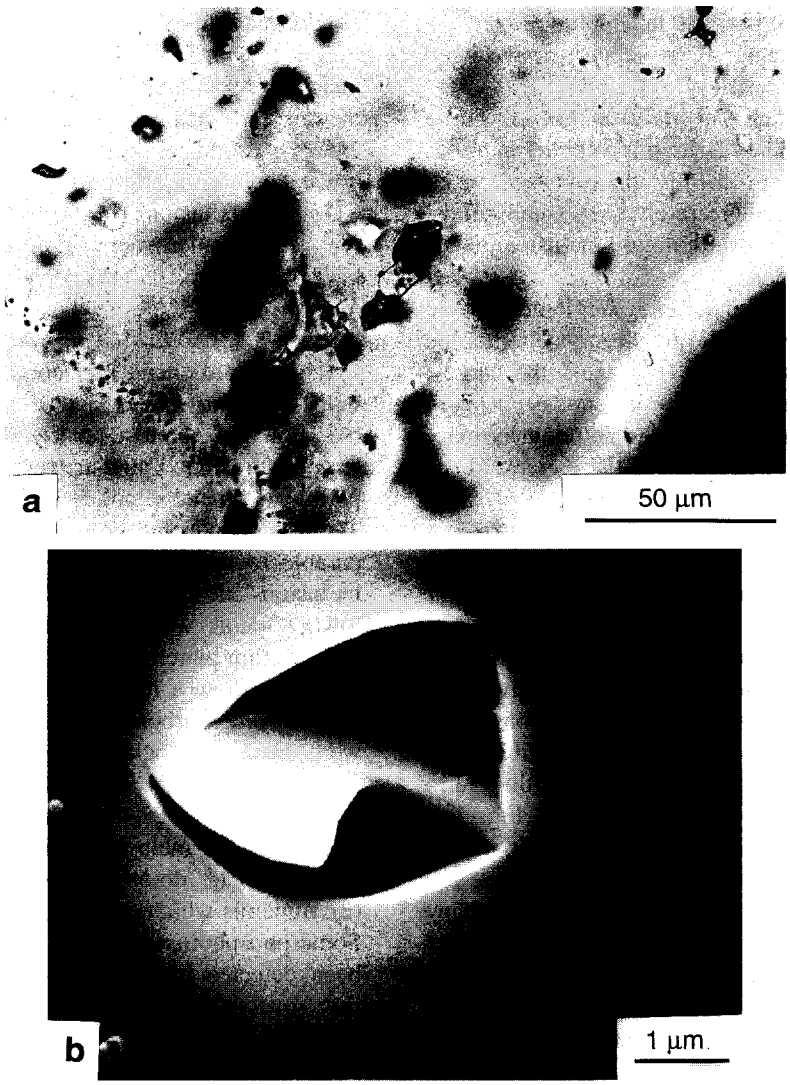

Fig. 4. Type 2 solid-rich fluid inclusions in the 85ZA68-b sample. (a) Plane polarized microphotograph of a solid-rich fluid inclusion showing the shrunk vapour bubble and the multiple solids. (b) S.E.M. microphotograph showing an open solid-rich fluid inclusion containing daughter minerals.

1981; Roedder, 1984). In the Zabargad gneisses the following cross-cutting relationships have been observed. (1) Where a plane of regular or large decrepitated type 1a CO_2-fluid inclusions and a plane of small type 2 solid-rich aqueous fluid inclusions intersect, the type 1a CO_2-fluid is replaced by the solid-rich aqueous fluid in the cavities localized at the intersection. Here the solid-rich aqueous fluid is younger than the CO_2-fluid. (2) Where a plane of large irregular vapour-rich type 1b CO_2-fluid inclusions and a plane of small type 2 solid-rich aqueous fluid inclusions intersect, it can be seen that small crystals are incorporated within the large CO_2-fluid inclusions. In this case, the vapour-rich CO_2-fluid inclusion plane is younger than the solid-rich aqueous fluid inclusion plane.

The fact that only irregular vapour-rich CO_2-fluid inclusions are present in scapolites suggests that type 1b vapour-rich CO_2-fluid inclusions occur later than scapolite crystallization in metagabbros.

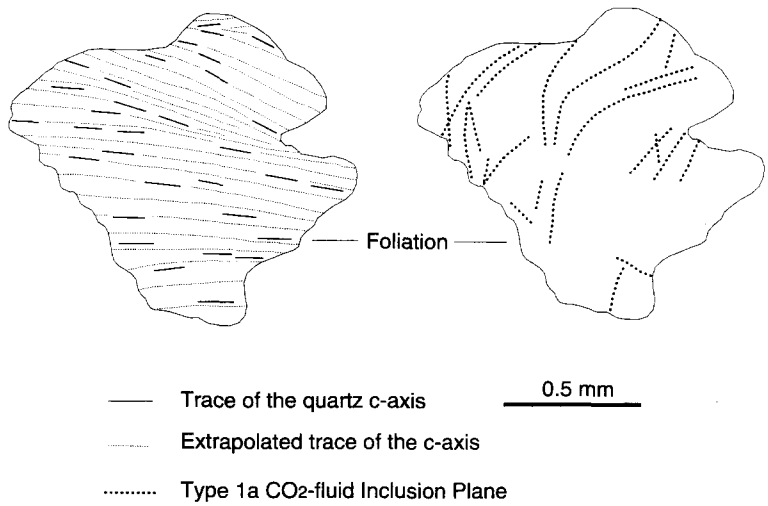

Fig. 5. Type 1a CO_2-fluid inclusion planes distorted together with the quartz crystallographic lattice in the 85ZA68-a sample. Drawing from a microphotograph.

Concerning the relationship between the fluid inclusions and the deformation textures in the rock, it has been quoted in the previous sections that type 1a CO_2-fluid inclusions are observed in quartz grain boundaries. Consequently, CO_2 was introduced in the rocks prior to the last plastic deformation and dynamic recrystallization of quartz. This is particularly clear for the CO_2-fluid inclusions displaying a regular shape or decrepitation halos. The planes of this type 1a CO_2-fluid inclusions are rotated within the quartz crystals following the same pattern as the quartz crystallographic lattice (Fig. 5). The planes of solid-rich aqueous and vapour-rich CO_2-fluid inclusions are not deformed, suggesting therefore that they occur later than the last plastic deformation.

In the 86ZA34-b gabbro, the CO_2-fluid inclusion planes are not rotated and scapolites are undeformed. The last plastic deformation which is observed in the 85ZA68 granulites s.str. in the quartz ribbons either did not occur at that place or, more probably, was too weak or of a too low temperature to be registered by plagioclase-rich rocks such as 86ZA34-b.

4.4. Orientation of the fluid inclusion planes

As mentioned above, the fluid inclusion planes are healed microcracks. Moreover, several authors (Tuttle, 1949; Wise, 1964; Tapponnier and Brace, 1976; Boullier, 1982; Lespinasse and Pêcher, 1986) have demonstrated that they are mode I microcracks which occur in the σ_1–σ_2 plane (orthogonal to σ_3) and therefore, their orientation may be correlated to that of the stresses at the time of their creation. Thus, the orientation of fluid inclusion planes has been measured in the Zabargad gneisses in order to bring some information on the stress orientation or stress changes during the fluid percolation.

The host mineral of the microcracks, the type (type 1a or 1b CO_2-fluid or type 2 solid-rich aqueous fluid), texture (decrepitated or not) and size of fluid inclusions within the microcracks (less than 1 μm, 1 μm and 2–5 μm average diameter) have been noted in order to present distinct stereograms for poles of different types of microcracks. It has to be noted that, because of the uncertainty of measurement of the orientation of largest fluid inclusions in plagioclase, most of the planes measured in this mineral concern $\leq$ 2 μm fluid inclusions. Stereograms have been contoured using Stereoplot software (version 3, N. Mancktelow, 1995, ETH Zürich).

In the granulites s.str. (Figs. 6 and 7). Type 1a CO_2-fluid inclusion planes are not randomly oriented respective to the strain axes (lineation X, foliation XY) defined by the granulite-facies minerals and show a lack of poles in the centre Y of the stereograms in both samples (85ZA68-b and 85ZA-68-a), that is a lack of planes normal to the foliation and containing the stretching lineation. The general

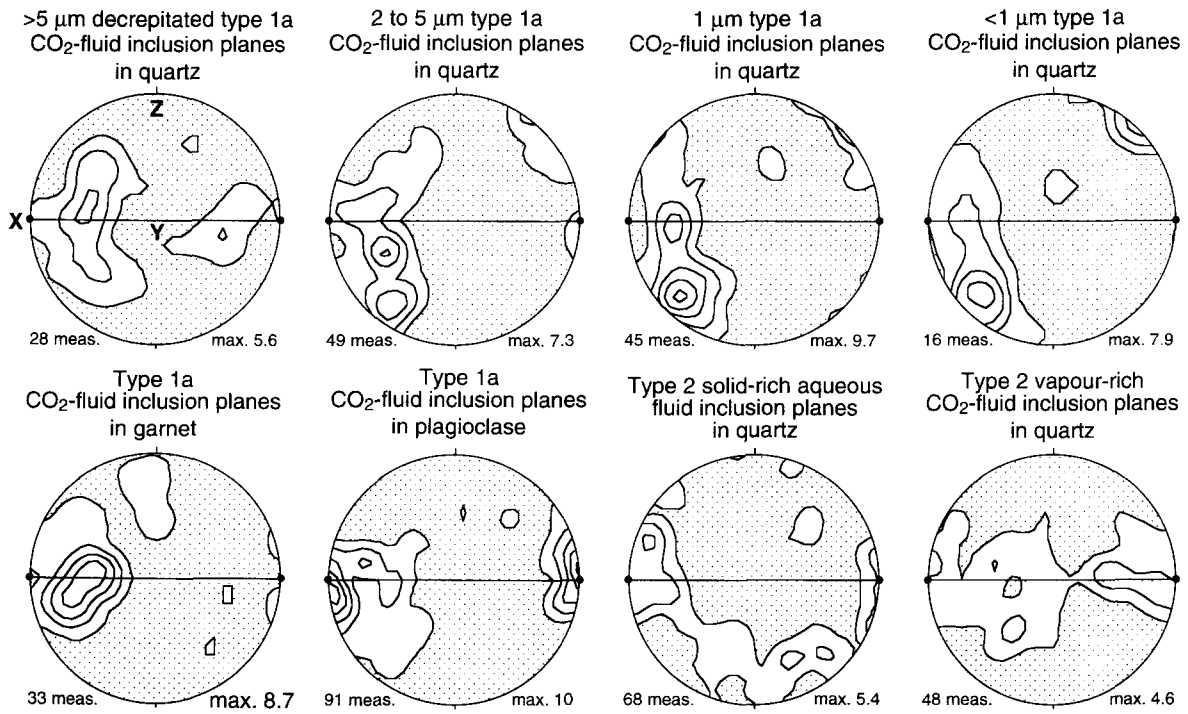

Fig. 6. Contour diagrams (1, 3, 5, 7 ... multiples of uniform distribution) of the poles of fluid inclusion planes in sample 85ZA68-b. Lower-hemisphere projection. Foliation is E–W vertical and lineation E–W horizontal. Number of measurements and maximum concentrations are indicated.

tendencies of these stereograms are the following: type 1a fluid inclusion planes tend to be at a high angle to the foliation plane and at a high (in plagioclase) or intermediate (in garnet and quartz) angle to the lineation. In quartz, some gradation may be seen in the orientations with decreasing size of fluid inclusions: planes of large fluid inclusions are at an intermediate angle to the lineation and the smallest fluid inclusions are at a high angle to that direction. This is particularly clear in the 85ZA68-a sample (Fig. 7), where the poles of <1 μm fluid inclusion planes are close to the lineation and similarly oriented as fluid inclusion planes in plagioclase (≤ 2 μm in diameter). It should be noted also that the distribution maxima are generally slightly oblique to foliation and lineation, thus suggesting a rotational component for the deformation.

Type 2 solid-rich aqueous fluid inclusion planes have a remarkably different orientation at least in the 85ZA68-a sample where they are parallel to the lineation and perpendicular to the foliation (poles near the centre of the stereogram). In the 85ZA68-b sample, the poles define an outer girdle on the stereogram, i.e. the planes are 'en zone' with the *Y* axis.

Taking into account the number of measurements possible in both samples (only 12 measurements in 85ZA68-a), type 1b fluid inclusion planes are broadly oriented normal to the foliation but randomly oriented relative to the lineation (poles in a girdle parallel to the foliation plane).

In the 86ZA34-b gabbro (Fig. 8). Only one ordinary *XZ* thin-section of the 86ZA34-b gabbro was available which was used previously for geochemical analysis. Therefore, only 2D measurements have been performed. Only qualitative estimations of dips of fluid inclusion planes were possible. However, it may be seen that type 1a CO_2-fluid inclusion planes are oriented at high angle to the foliation (Fig. 8) and to the stretching lineation in this facies. As for stereograms of type 1a CO_2-fluid inclusion planes in granulites s.str., rose diagrams show an oblique distribution of fluid inclusion planes relative to the

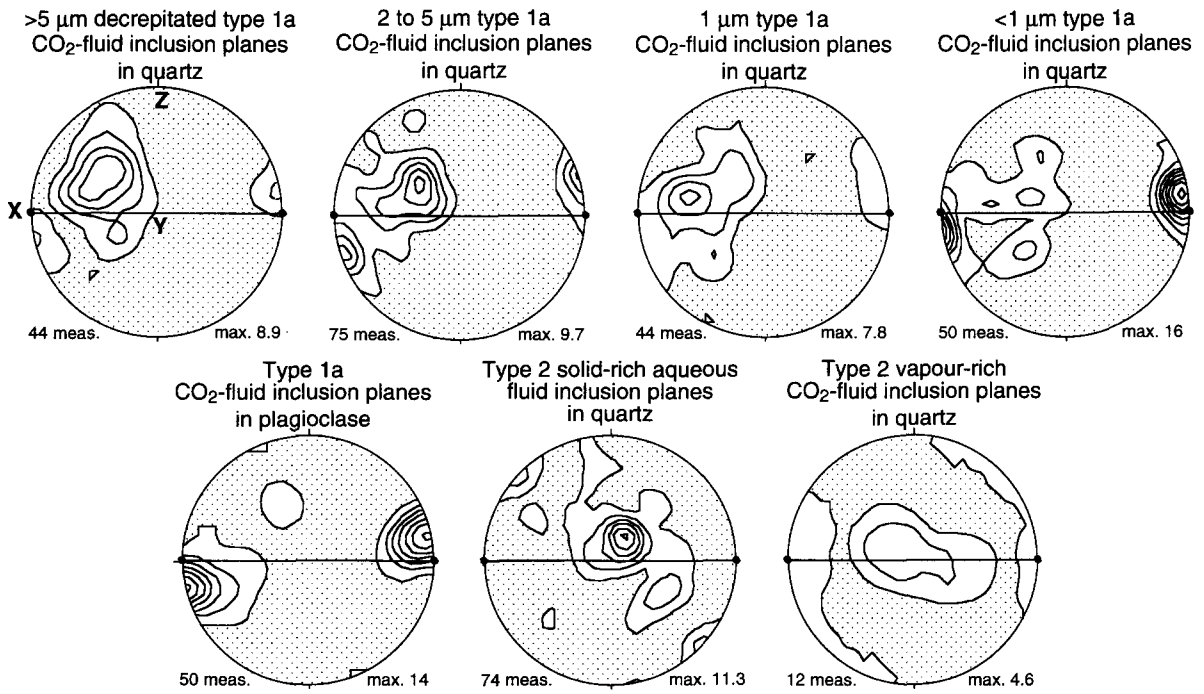

Fig. 7. Contour diagrams (1, 3, 5, 7 ... multiples of uniform distribution) of the poles of fluid inclusion planes in sample 85ZA68-a. Lower-hemisphere projection. Foliation is E–W vertical and lineation E–W horizontal. Number of measurements and maximum concentrations are indicated.

lineation and foliation, suggesting also a rotational component of the deformation. On the other hand, the type 2 solid-rich aqueous fluid inclusion planes are lying approximately within the *XZ* finite strain plane (subparallel to the thin-section). This type of orientation was found also in amphibolites.

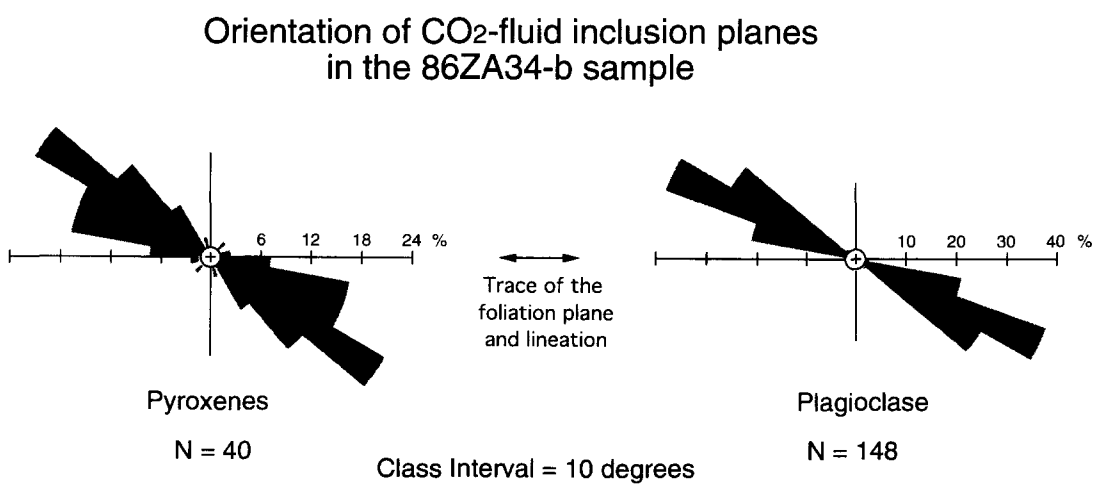

Fig. 8. Rose diagrams showing the orientation of poles of type 1a CO_2-fluid inclusion planes at high angle to trace of the foliation plane and to the lineation (horizontal) in sample 86ZA34-b.

4.5. Microthermometric data

As fluid inclusions were similar in 85ZA68-a and 85ZA68-b, only one thick doubly polished section of the 85ZA68-b sample was used for detailed microthermometric measurements in order to deduce the P–V–T–X properties of the trapped fluids. Results are reported in Figs. 9 and 10.

Type 1 CO_2-fluid inclusions (Fig. 9). Several fluid inclusion planes were studied in detail in order to verify the consistency of phase-change temperature measurements within a single microcrack and within the whole sample. The microthermometry of fluid inclusions appears to be constant: all the melting temperatures (T_mCO_2) measured in a single type 1a or 1b microcrack or within different microcracks were −56.6°C. One clathrate melting temperature (T_mCl) was measured in the large irregular type 1b vapour-rich H_2O-bearing fluid inclusion (9.8°C). These results considered together indicate that type 1a and 1b fluid inclusions are filled with pure CO_2. This chemistry has been confirmed by M.C. Boiron using a Raman microprobe (CREGU, Nancy).

T_hCO_2 are comprised between 23.6°C to the liquid, 30.3°C to the critical and 3.1°C to the vapour phase (Fig. 9). No T_hCO_2 to the liquid lower than 23.6°C has been measured. The scatter of T_hCO_2 is generally less than 1°C in a single type 1a microcrack, except for large decrepitated and large irregular vapour-rich CO_2-fluid inclusion planes which may display up to 5°C scattering of T_hCO_2 to the liquid and 17°C to the vapour, respectively.

Some type 1a fluid inclusions located within quartz grain boundaries were large enough to be investigated. As all the other CO_2-fluid inclusions, their T_mCO_2 is that of pure CO_2 (−56.6°C) and their homogenization temperature is close to 25°C (Fig. 9).

Solid-rich aqueous fluid inclusions (Fig. 10). These fluid inclusions did not react during cooling (down to −180°C). No ice could be seen, perhaps due to the large number of solids within the inclusions. The determination of the nature of the large vapour phase in these fluid inclusions with the Raman mi-

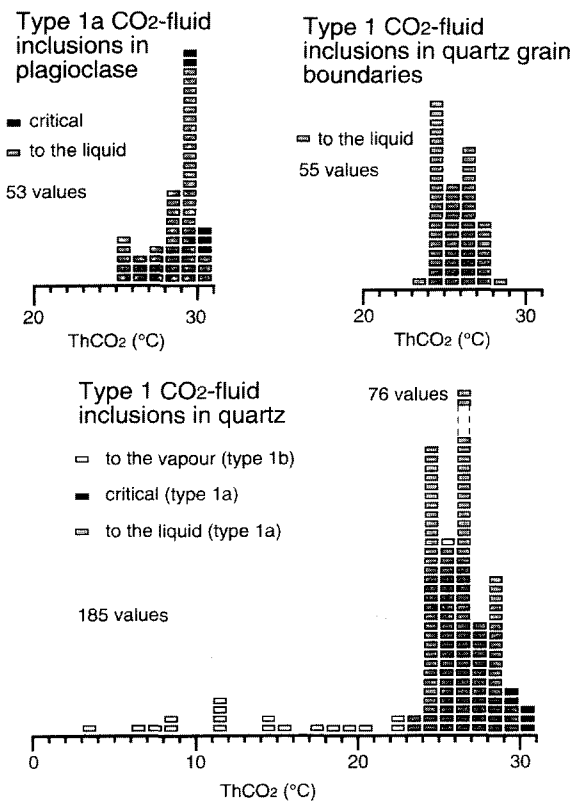

Fig. 9. Microthermometric data for type 1 CO_2-fluid inclusions within the healed microcracks in plagioclases, the recrystallized quartz grain boundaries and the healed microcracks in quartz grains. Homogenizations to the liquid, critical or vapour are indicated.

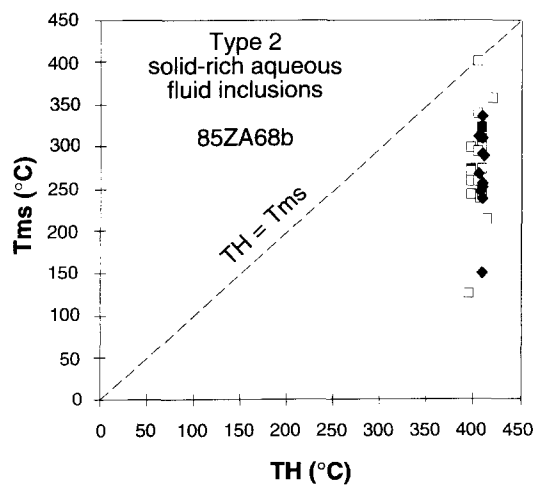

Fig. 10. Microthermometric data for type 2 solid-rich fluid inclusions. T_{ms} is the temperature of disappearance of the solid and TH is the temperature of disappearance of the vapour bubble. The different symbols correspond to measurements performed in different microcracks.

croprobe (M.C. Boiron, CREGU) indicates that they are highly saline aqueous fluid inclusions with no other volatile component than water in the vapour phase. During heating, dissolution of the solids was observed in a large interval of temperature (T_{ms} from 124° to 401°C, Fig. 10). Total homogenization by disappearance of the vapour into the liquid phase (T_h) generally occurs above 400°C (from 396° to 423.7°C, 23 measurements). In some fluid inclusions, a solid remained above the homogenization temperature and did not disappear after heating to 450°C. Therefore, it is suggested that this particular solid is not a daughter crystal precipitated from the highly saline fluid but was trapped together with that fluid.

4.6. P–V–T–X properties of the fluids

Thermometric data were interpreted in terms of composition and density of the trapped fluids. Calculation of the isochoric (isodensity) lines were performed with MacFlinCor software (Brown and Hagemann, 1994) using the state equation of Jacobs and Kerrick (1981) for CO_2-inclusions and of Bowers and Helgeson (1983) for the one observed type 1b H_2O-bearing CO_2-inclusion. Because of their complexity (high content and variability of solids), the solid-rich aqueous fluid inclusions were assimilated to H_2O–NaCl fluid for simplification and their microthermometric data ($250°C < T_{ms} < 350°C$; $T_h \approx 400°C$) are interpreted, by default of more precise knowledge of the system, using the P–V–T–X representation of the H_2O–NaCl system with 40 wt.% NaCl studied by Bodnar and Vityk (1994) and Bodnar (1994). The disappearance of the vapour phase ($T_h \approx 400°C$) in these inclusions gives us an indication of the minimum trapping temperature of these highly saline fluids.

The calculated isochores for type 1 and 2 fluid inclusions are shown in Fig. 11 as well as other information available on the crustal rocks from Zabargad, which will be discussed in the next sections.

5. Interpretation

5.1. Petrography and fluid inclusion chronology

Petrographic examination of the above samples and comparison with those described by Bonatti and Seyler (1987), Seyler and Bonatti (1988) and Boudier et al. (1988) allow to reconstruct the P–T history of the Zabargad gneisses. The garnet–pyroxene–plagioclase geobarometer (Perkins and Newton, 1981) applied to the first granulite-facies assemblage of the 85ZA68-b sample indicates pressure conditions of 1.08 GPa for a given temperature of 850°C (Boudier et al., 1988). In the 86ZA34-b gabbro, the Wells (1977) geothermometer indicates a temperature around 850°C corresponding to the last equilibration of the two-pyroxene porphyroclasts (Boudier et al., 1988; stage I, Fig. 11).

The second assemblage in the 85ZA68-b quartz-bearing mafic granulite results from the reaction:

garnet + quartz = orthopyroxene II + plagioclase

which is typical of an isothermal decompression path (Harley, 1989). In the 86ZA34-b gabbro, the Wells (1977) geothermometer indicates a temperature of 895°C for recrystallized pyroxenes and the mylonitic deformation textures in this sample are significative of a high temperature (750–950°C; Ji et al., 1988). During this deformation, high aluminium-content pyroxenes recrystallized into low aluminium-content pyroxenes, suggesting also a decrease in pressure between the first and second stages at a more or less constant temperature (ca. 850°C). It was not possible to determine the pressure from the mineral assemblages of the samples studied in this paper. However, Seyler and Bonatti (1988) have estimated the pressure conditions for this second stage at ca. 500 MPa in the mafic granulites and a maximum of 650 MPa pressure in the felsic granulites (stage II, Fig. 11).

After the second stage, the Zabargad gneisses have been plastically deformed (stage IV) and then hydrated at a lower temperature (stage V). As suggested by the small size of the recrystallized quartz grains and by the width of the quartz subgrains, this deformation should have occurred under high stress or low temperature (Nicolas and Poirier, 1976). No superimposed structures were observed on the granulite-facies lineation and foliation. Therefore, it is suggested that both the deformation during isothermal decompression (stage I to stage II) and the last plastic deformation of quartz (stage IV) were at least coaxial if not belonging to a deformation continuum. Temperature of the subsequent hydra-

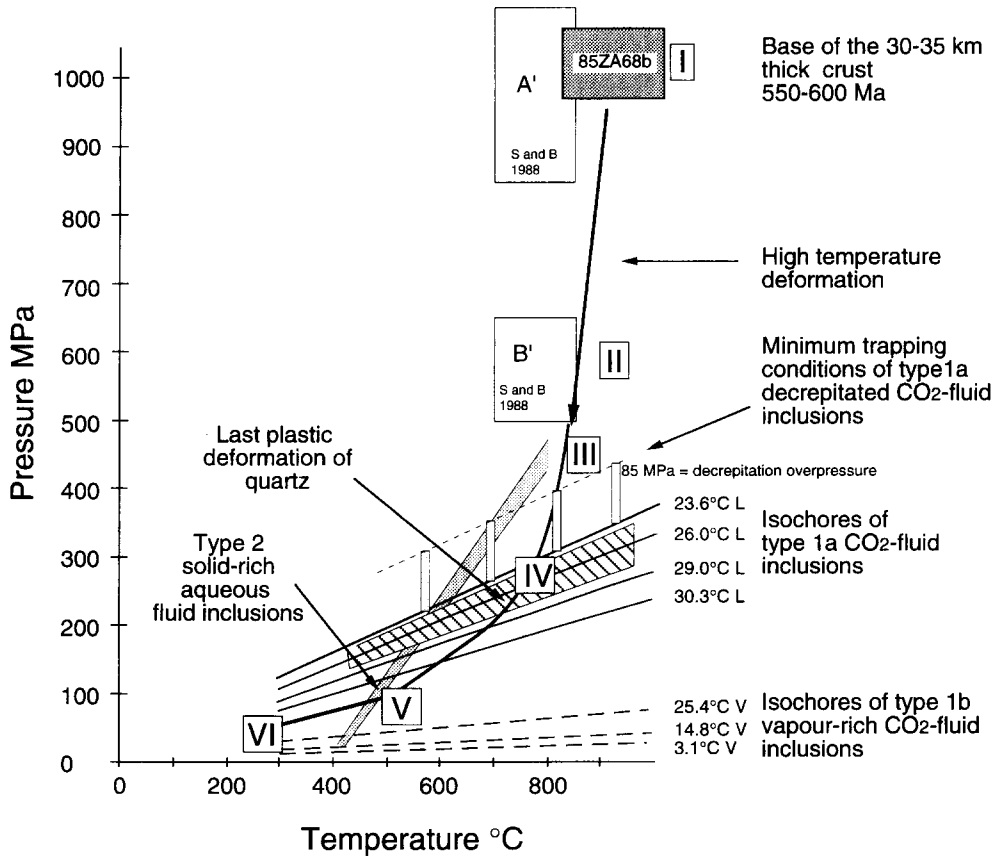

Fig. 11. *P–T* path of the Zabargad gneisses based on fluid inclusion data (isochoric lines) and textures from the 85ZA68-b sample. Stages I to VI are described and discussed in the text. Boxes *A'* and *B'* are those proposed by Seyler and Bonatti (1988) for the two granulitic assemblages in the sialic gneisses. The other box is from the *P–T* determination by Boudier et al. (1988) for the 85ZA68-b granulite.

tion process was estimated to be at least 500–700°C in tectonized amphibolites near the contact between the gneisses and the peridotites by Boudier et al. (1988), and between 600° and 740°C and $P < 200$ MPa in the sialic gneisses by Seyler and Bonatti (1988). Additional *P–T* constraints will be imposed later using fluid inclusions. The products of hydration of granulites (green or colourless amphiboles, kelyphyte around garnet) have no preferred orientation; consequently, it is concluded that they postdate the last deformation and dynamic recrystallization of quartz. As temperature of hydration is relatively high (> 500°C), this implies that the last plastic deformation of quartz has occurred under high strain rate rather than under low temperature.

From the observation of fluid inclusions in relation to textures, it was concluded that all fluid inclusions are secondary, i.e. they postdate the crystallization of minerals. Type 1a CO_2-fluid inclusions were trapped first. The minimum pressure conditions for trapping of these fluids may be determined by the large decrepitated fluid inclusions which have undergone at least 85 MPa of internal overpressure as experimentally calibrated by Leroy (1979) and Sterner and Bodnar (1989). This minimal overpressure has to be added, therefore, to the highest isochoric line corresponding to the lowest value of T_hCO_2 to the liquid measured in decrepitated CO_2-fluid inclusions (+23.6°C). From the crack length/inclusion diameter, the strong spatial relationships between large and small type 1a CO_2-fluid inclusions and the constant composition of these fluid inclusions (pure CO_2), it may be deduced that most of the CO_2-fluid inclusion planes result from the decrepitation of the

firstly trapped CO_2-inclusions rather than from an income of carbonic fluid over a long period of time. Such relationship has been previously observed in metamorphic rocks from the Himalayas which have followed a nearly isothermal decompression path (Boullier et al., 1991).

Preferred orientations of the type 1a fluid inclusion planes show that these microcracks are in some way related to the strain axes defined by the granulite-facies minerals and by the quartz ribbons. This is clear for type 1a fluid inclusion planes in plagioclase (85ZA68-a and -b) and in plagioclase and pyroxene (86ZA34-b) where they are consistent with an extension in the X direction as defined by the stretching lineation. Petrographic observations (bending of fluid inclusion planes and type 1a CO_2-fluid inclusions within grain boundaries) clearly demonstrate that type 1a CO_2-fluid inclusion planes were affected by the last plastic deformation of quartz (stage IV). T_hCO_2 of CO_2-fluid inclusions within quartz grain boundaries (23.6 to 28.3°C) have intermediate values between that of decrepitated CO_2-fluid inclusions (23.6°C) and that of the lowest density type 1a CO_2-fluid inclusions (30.3°C to the critical). Therefore, it is suggested that the largest type 1a CO_2-fluid inclusions were trapped at the end of or after the high-temperature deformation and have decrepitated during and slightly after the last plastic deformation of quartz. The P–T path of the Zabargad gneisses is thus constrained by the low slope isochoric lines of the CO_2-fluid inclusions contemporaneous with the late plastic deformation of quartz (stage IV, Fig. 11). The oblique orientation of the type 1a CO_2-fluid inclusion planes relative to the lineation suggests also a shear component for the last plastic deformation. It has to be noticed that the shear sense deduced from the high-temperature deformation (Ji et al., 1988; Boudier et al., 1988) is identical to that deduced from the obliquity of fluid inclusion planes on lineation (86ZA34-b), that is fluid inclusion planes are subparallel to the shortening direction. That reinforces the idea of a deformation continuum including the high-temperature deformation and the last plastic deformation of quartz.

A change in the stress orientation and in the nature of the percolating fluid occurred after the last plastic deformation of quartz. This is shown by the trapping of type 2 solid-rich aqueous fluid inclusions in microcracks with different orientation relative to the foliation and lineation of the gneisses compared to that of type 1a. These type 2 fluid inclusions are very similar in aspect to the hypersaline fluid inclusions described by Clocchiatti et al. (1981) and Kurat et al. (1993) in the peridot gemstones located below the large dolerite sill intruding the southern peridotite body. But the major difference is in the nature of the volatile component which is aqueous in the gneisses and CO_2 and/or N_2 without H_2O in the peridot gemstones where these hypersaline fluids were probably derived from peridotite reservoirs (Kurat et al., 1993). In the gneisses, the hypersaline fluid may have derived from percolating seawater modified by the extensive hydration of the gneisses and amphibolites, but they may also result from leaching of the Middle Miocene evaporites. Whatever the origin of these fluids, the P–T path should fit the minimum trapping temperature for the solid-rich aqueous fluid inclusions (around 400°C) and their isochoric lines drawn after the experimental data of Bodnar (1994). They were trapped at stage V (Fig. 11) after the dense carbonic fluid inclusions (homogenization to the liquid) but prior to the low-density vapour-rich carbonic fluid inclusions (homogenization to the vapour).

Another change occurred in stress orientation during trapping of type 1b vapour-rich CO_2-fluid inclusion planes (stage VI) which orientation suggests a pure shear regime (coaxial flattening) in which σ_2 and σ_3 were almost equal in the horizontal plane (nearly subhorizontal foliation). However, and because type 1a- and 1b-fluid inclusions are pure CO_2, a decrepitation process of large and dense type 1a into vapour-rich type 1b CO_2-fluid inclusions may be proposed rather than an influx of a new fluid through the gneisses.

A similar fluid chronology was observed in a euhedral quartz crystal kindly provided by H. Brueckner and coming from a hydrothermalized zone within the gneiss unit. In this crystal, the oldest fluid inclusions are pseudosecondary CO_2-rich fluid inclusions trapped within cracks formed during crystal growth (Roedder, 1984) and showing a thin meniscus of water against the fluid inclusion walls. These fluid inclusions show ca. 0.8 filling ratios (large CO_2 vapour bubble). The latest fluid inclusions are secondary H_2O–NaCl-saturated fluid inclusions. In this

sample, some mixing has occurred between the two types of fluids giving intermediate CO_2–H_2O–NaCl fluid inclusions.

5.2. Time constraints on the P–T–t path

Some geochronological data are available on rocks from Zabargad Island and surrounding areas. They are summarized in the following section. Unfortunately, it is not yet possible to date directly fluid inclusions in rocks and, therefore, timing of fluid inclusion trapping will be only constrained by correlations with structures which are in turn interpreted in terms of geological events. These correlations based on interpretations are, therefore, destined to be discussed.

The Zabargad gneisses clearly represent the deep Pan-African continental crust since minerals of the first granulitic assemblage (stage I, Fig. 11) in the 85ZA68-b granulite give a Pan-African age on a Sm–Nd isochron diagram (whole rock, clinopyroxene and garnet; 548 ± 10 Ma, Lancelot and Bosch, 1991). This age is slightly younger than that of a felsic granulite studied by the same authors (669 ± 34 Ma, whole rock, orthopyroxene and garnet Sm–Nd isochron; 665 ± 8 Ma, whole rock, orthopyroxene and garnet Rb–Sr isochron). Brueckner et al. (1995) have obtained a Sm–Nd isochron of 552 ± 4 Ma and an age of 695 ± 2 Ma by evaporation of zircon grains on similar felsic gneisses, thus confirming the Pan-African age of the continental crust equilibrated under pressure and temperature conditions around 1.0 to 1.1 GPa and more than 850°C (Bonatti and Seyler, 1987; Boudier et al., 1988; Seyler and Bonatti, 1988). According to the average thickness of the stable continental crust (35 to 40 km; 32.5 km as determined by Le Pichon and Gaulier, 1988, for the Nubian continental crust prior to rifting), these *P–T* conditions as well as the presence of rooted peridotites in the immediate vicinity of the gneisses strongly suggest that Zabargad gneisses represent the base of the Pan-African continental crust close to the Moho as already proposed by Bonatti and Seyler (1987). The granulites have tonalitic–trondhjemitic affinities and, therefore, may be compared with the southern Kapuskasing uplift (Canada) which is known to be the base of an Archaean continental crust originated in magmatic arc environments (Percival, 1989). The Pan-African orogen of the Nubian and Arabian shields was formed in such an environment of accretion of island arcs and interleaving oceanic basins (Kröner et al., 1987).

The gabbroic intrusions were emplaced at the base of the continental crust (Bonatti and Seyler, 1987; Seyler and Bonatti, 1988) during stage I. Brueckner et al. (1995) obtained a whole-rock Sm–Nd model age of 638 Ma for a gabbro interpreted as the emplacement age. The base of the continental crust was submitted to a more or less isothermal decompression during a high-temperature deformation as suggested by the flattened assemblages of garnet, plagioclase and pyroxenes in the intermediate granulites (Fig. 2 and stage II in Fig. 11). The gabbros have also suffered this high-temperature deformation (Boudier et al., 1988; Ji et al., 1988) together with the sialic granulites during an isothermal decompression which may be explained either by an intense thinning of the crust (from 30–35 km to 15–20 km, Fig. 11) or by a tectonic emplacement of the granulites in the middle crust (Harley, 1989). Brueckner et al. (1995) obtained a cpx–plag–wr Sm–Nd isochron on a gabbro indicating an age around 70 Ma. Is this latter age significative of the recrystallization during the high-temperature deformation (stage II)? The question is still debatable. It has to be noted that in the 85ZA68-b mafic granulite where two generations of plagioclase coexist (stages I and II), at least the Rb–Sr system of plagioclase appears disturbed relative to the other minerals unless the age of the perturbation cannot be precised (Lancelot and Bosch, 1991). Moreover, plagioclase peridotites from the southern body display also perturbations of the Rb–Sr and Nd–Sm systems (Bosch, 1991; Brueckner et al., 1995) indicating that some event occurred in recent time (<90 Ma) which the authors relate to downward percolation of seawater into the peridotites. Therefore, no clear age constraint may be imposed for the second metamorphic stage (stage II on Fig. 11) and two different interpretations have been proposed. Following Brueckner et al. (1995), the high-temperature deformation of the gneisses and stage II are Pan-African in age, based on Sm–Nd isochrons on minerals from granulites and on alignment of peridotite Sm–Nd whole rocks on a SLAP line at 675 Ma. Following Boudier et al. (1988) this high-temperature deformation and stage

II are related to intense crustal thinning during the initiation of the Red Sea rift.

Diabase dykes are then intruded, transformed into amphibolites and deformed together with the gneisses near the contact with peridotites. This deformation occurred at temperatures around 500–740°C as determined by Boudier et al. (1988) and Seyler and Bonatti (1988) and corresponds to stage IV in Fig. 11. Nicolas et al. (1987) provided a 23 Ma K–Ar age on amphibole of a deformed and metamorphic dolerite dyke within the gneisses. Tholeiitic magmatism accompanying the early opening of the Red Sea occurred between 24 to 21 Ma ($^{40}Ar/^{39}Ar$, Féraud et al., 1991) and began once the Arabian crust had thinned to 20–25 km (Bohannon, 1989). Brueckner et al. (1995) obtained a younger, 17.5 Ma age on one diabase dyke by Re–Os method. Therefore, emplacement of diabase dykes and deformation of stage IV may be Early Miocene in age.

According to all the authors who have worked on Zabargad Island, the last metasomatism recognized in the gneisses (stage V) and in peridotites is clearly related to the Red Sea rift (Seyler and Bonatti, 1988; Boudier et al., 1988). Geochemical (Dupuy et al., 1991) and stable isotope data (Agrinier et al., 1993) on peridotites are interpreted by the authors as the result of penetration of seawater through hydrothermal systems. Trapping of type 2 solid-rich aqueous fluid inclusions is attributed to that stage. Depending on the origin of the hypersaline aqueous fluid, two different timings may be proposed for stage V. Following the first hypothesis correlating these fluid inclusions to the hypersaline CO_2/N_2 fluid inclusions observed in the peridot gemstones and attributed to thermal effect of the diabase dykes (Clocchiatti et al., 1981; Boudier et al., 1988; Boudier and Nicolas, 1991), the age of stage V is the age of the diabase dykes, i.e. 24 to 21 Ma (see above). But it may be slightly younger, since zircons with probable hydrothermal origin and which were collected near the central peridotite body, have provided subconcordant Pb–Pb ages of 19 to 21 Ma and upper- and lower-intercept U–Pb discordia ages of 143 and 18.4 Ma, respectively (Oberli et al., 1987). Thus, following the first hypothesis, stage V may be Early Miocene in age (24 to 18 Ma). Following the second hypothesis deriving these fluid inclusions from leaching of evaporites by seawater, as suggested by Clocchiatti et al. (1981) in order to explain the origin of salts in the inclusions of peridot gemstones, the brines may be younger than the discordant and undeformed evaporite unit of Zabargad Island which is Middle Miocene in age (Bonatti et al., 1983), i.e. between 16 and 11 Ma. A comparison could be made with salt-enriched aqueous fluid inclusions observed by Ramboz et al. (1988) in epigenetic anhydrite from the Atlantis II Deep (southern Red Sea) and which display a salinity up to 33 wt.% equiv. NaCl and a T_h around 400°C. Trace element geochemistry and especially Br/Cl and I/Br ratios could provide also some informations on the origin of the highly saline fluids in the Zabargad gneisses as it has been performed in other geological contexts (Munz et al., 1995).

6. Discussion

The time constraints on the P–T path of the Zabargad gneisses may be explained by two geodynamic models which mainly differ by the age of stages II (low-pressure granulite facies metamorphism) and III (trapping of the first CO_2 fluid inclusions), and which are described below.

6.1. Model 1

Brueckner et al. (1988, 1995) proposed that gneisses have been extracted from a depleted mantle during the Pan-African orogeny at ca. 695 Ma. Then, the gneisses and peridotites shared a common history, were juxtaposed (stage I) and brought to near the surface during the Pan-African orogeny (stage II). They subsequently suffered a hydrothermal event, leading to the formation of the plagioclase-rich assemblages in the southern peridotite body (troctolites of Brueckner et al., 1988) and of the peridot gemstones, which may have occurred during the Miocene or post-Miocene, or as long ago as the Early Cretaceous. In this model, stages I, II and III (and may be IV) are Pan-African, and only stages V and VI are related to rifting. Following this point of view, the CO_2 fluid (stage III) was trapped during the granulite facies metamorphism as commonly observed in granulites of various ages (Touret, 1987) and especially in Pan-African granulites from eastern Africa (Coolen, 1980) or Sri Lanka and southern India (Santosh, 1986; Santosh et al., 1991). The CO_2

fluid trapped in the euhedral quartz from a hydrothermal zone in the gneisses could be originated from the thermal metamorphism and metasomatism of the Zabargad Formation and, therefore, have a different origin than the CO_2 fluid inclusions in the granulites (H.K. Brueckner, pers. commun., 1996). These two different CO_2 metasomatisms were separated by about 550 Ma.

6.2. Model 2

Boudier et al. (1988) have proposed a model in which stage I alone is Pan-African, and the other stages are related to Red Sea rifting. Following these authors, the gneisses, gabbros and peridotites represent the base of the Pan-African 30–35 km thick continental crust (stage I). All these rocks were subsequently co-structured during the ascent of the peridotites which belonged to an asthenospheric diapir and induced thinning and shearing of the crust during the early stage of the Red Sea rift formation (850°C and 600 MPa, i.e. 20–25 km thick crust). During a continuing ascent, the temperature decreased producing amphibolites from numerous basaltic dykes originated by melting of the diapir. The shear zone located at the contact between the peridotites and the gneisses favoured seawater penetration and induced hydration of the gneisses and hydrothermal formation of the peridot gemstones. Following this model, the interface between the gneisses and the peridotites is young and represents the tectonized intrusive contact of the diapir into the deep Pan-African continental crust.

Our preference is for the second model, but with some variations on the theme in order to take into account the isotopic results from Brueckner et al. (1995) and geothermobarometry on peridotites by Kurat et al. (1993) who show that the various facies of peridotites from Zabargad plot on a high geothermal gradient ranging from 1280°C and 2700 MPa to 870°C and 300–500 MPa. The evidences that led Nicolas et al. (1987) to infer an asthenospheric diapir in Zabargad Island, are the continuity of the peridotites between the three massifs and with the mantle beneath the Red Sea as shown by geophysical data (Styles and Gerdes, 1983), the high-temperature deformation in the southern and central peridotites and the evidences of partial melting in these massifs. Structural studies (Nicolas et al., 1987) suggested that the Zabargad peridotites represent the western limb of a diapir wall parallel to the Red Sea rift and that the asthenospheric flow was moving upward toward the southeast. Actually, these structures may be interpreted in a slightly different way as already proposed by Dupuy et al. (1991): in spite of representing the diapir itself, the northern and central peridotite bodies may represent the continental lithosphere attached to the crust and intruded by an asthenospheric diapir (southern body) centred on the southeast of Zabargad Island (Styles and Gerdes, 1983). The high-temperature deformation of the northern and central spinel peridotites could reflect rather a mechanical and thermal effect of a hot neighbouring ascending diapir than deformation within the asthenospheric diapir itself. This could reconcile the isotopic data of Brueckner et al. (1995), dating the interface between the peridotites and gneisses as Pan-African, with petrographical and structural observations (Boudier et al., 1988; this work). In that case, this interface would represent the Pan-African Moho somewhat subsequently modified by deformation. It would explain also the different trace element and isotopic signatures of plagioclase peridotites from the southern body (Dupuy et al., 1991; Brueckner et al., 1995).

The first deformation registered by the gneisses and gabbros is the high-temperature deformation separating high-pressure (stage I) from medium-pressure (stage II) granulite facies metamorphism. Besides the structural evidences, assignment of that deformation to a rift-related uplift due to crustal thinning is supported by the perturbation of the Sm–Nd system in plagioclase peridotites of the southern body at 90 Ma or less, and by the 70 Ma age obtained by Brueckner et al. (1995) on a Sm–Nd isochron plot of minerals from a gabbro; as quoted in a previous section, this could be the age of dynamic recrystallization. The high temperature (750–950°C; Ji et al., 1988) may have been higher than the closing temperature of the Sm–Nd isotopic system allowing resetting of minerals during recrystallization (Mezger et al., 1992). Moreover, it does not seem realistic that deformation textures in gneisses and gabbros could have survived at such high temperatures (around 800°C) since Pan-African time without annealing and recrystallization as expected in the

model of Brueckner et al. (1995), and the preservation of the deformation textures suggests that they were 'quenched' by a subsequent rapid uplift.

Two origins may be invoked for the CO_2 fluid trapped during stage III. First, CO_2 may have been ancient and already trapped in granulites as very dense metamorphic fluid inclusions which decrepitated all along the isothermal decompression path followed by the gneisses (from stages I to IV). Second, CO_2 may have been derived from the mantle through partial melting and degassing of the ascending diapir below the thinned continental lithosphere, and may have been trapped during the early stages of rifting (III), but before the emplacement of diabases as no CO_2 fluid inclusions have been observed in the amphibolitized diabases. Unfortunately, there is no unambiguous way to distinguish between these two possible origins. Whatever the origin of this CO_2 fluid, the orientation of type 1a CO_2 microcracks is consistent with the flattening and the stretching directions indicated by the granulitic assemblage (nearly vertical N–S-striking, normal to the E–W-striking stretching lineation). This direction is slightly oblique to the opening direction of the Red Sea but is more or less parallel to the coast line near Zabargad Island (Sultan et al., 1993). Therefore, the formation of type 1a CO_2 microcracks may be integrated in the Red Sea rifting history.

If a continuum of deformation is envisaged between stages I and IV, model 2 proposed in this paper implies an important stretching of the continental crust because pre-rift (Zabargad Formation), syn-rift (evaporites) and post-rift sediments (coral reefs) are preserved at the same topographic level as the Moho, and constraints imposed to the P–T path by microthermometry on fluid inclusions implies an isothermal decompression (800 MPa) of the gneisses. This is in agreement with models of Le Pichon and Gaulier (1988) and Bohannon (1989) which proposed an important pre-rift extension of the continental crust during a 30 to 13 Ma period. Thinning of the crust occurred during high-temperature deformation (stage I to II) but also during medium-temperature deformation expressed by the amphibolitized diabases. K–Ar results on amphibole from one of these rocks indicate a 23 Ma age (Nicolas et al., 1987), thus dating stage IV.

The present study allows to estimate the minimum temperature and depth at which the type 2 hypersaline aqueous fluids were trapped (450°C and 100 MPa, i.e. ca. 3.7 km). These conditions indicate a very high geothermal gradient (around 100°C/km) if correlated to lithostatic fluid pressures, but slightly lower if fluid pressure is nearly hydrostatic as it is highly probable in an active extensional context (Sibson, 1990). Anyway, such high geothermal gradient is confirmed by the very low density of vapour-rich carbonic fluid inclusions postdating the solid-rich FI and is consistent with an oceanic accretion in the vicinity of Zabargad Island (see Le Pichon and Gaulier, 1988) which is located near the limit of the Red Sea oceanic crust (Bonatti and Seyler, 1987).

7. Conclusions

Samples of acidic, intermediate, and mafic granulitic gneisses from Zabargad Island (Red Sea rift) have been studied for their fluid inclusions in relation to their textures. The gneiss samples were collected at a maximum distance of 60 m above the contact with mantle peridotites with which they are co-structured by a high-T plastic deformation during an isothermal decompression starting from conditions estimated at 35 km depth and 850°C (stage I, base of the Pan-African crust). A first metasomatism of the crustal section during decompression is represented by CO_2-fluid inclusions trapped in all recrystallized phases at minimum conditions of 15 km depth and 800°C. Their origin is controversial: either a mantle source found in partial melting and degassing of asthenospheric mantle below the thinned lithosphere, or Pan-African CO_2, contemporaneous with the granulite facies metamorphism and already present in the gneisses before the isothermal decompression. The CO_2-fluid inclusion planes are controlled in orientation by the high-T plastic flow structures, but have been subsequently deformed during medium-T plastic deformation in quartz.

The second metasomatism is represented by solid-rich aqueous fluid inclusions which were trapped at minimum P–T conditions of 3.7 km depth and 450°C corresponding to a very high thermal gradient. They trace the introduction either of seawater or of fluids resulting from leaching of the Middle Miocene evaporites, within the gneisses during their residence at a shallow depth below the seafloor. They are

tentatively correlated with the formation of olivine gemstones (Clocchiatti et al., 1981) and type III amphibole in the peridotites (Dupuy et al., 1991; Agrinier et al., 1993; Kurat et al., 1993).

Two models are proposed in the literature. The first (Brueckner et al. (1995) suggests that most of the decompression P–T path is Pan-African in age and only the aqueous metasomatism is related to the rifting history of the Red Sea. The second (Nicolas et al., 1987; Boudier et al., 1988) supposes the existence of an asthenospheric diapir intrusive through the deep Pan-African crust leading to a continuous deformation event. In the latter, both metasomatisms are related to the Red Sea rifting history. Although it is impossible to date the trapping of fluid inclusions and to know with certainty the origin of the fluids, our preference is for the second model but slightly modified. The high-T decompression path traced by CO_2-fluid inclusions, relayed by solid-rich aqueous inclusions, and their respective minimum depths of equilibrium, trace a continuous process of crustal thinning of which fluid inclusions record the last stages. Such a continuous path would assign to a single event the thinning and uplift of the deep crust and uppermost lithosphere to shallow basin bottom during the Red Sea early rifting. In such an interpretative model, the northern and central peridotite bodies are representative of the uppermost continental lithosphere and only the southern body could belong to an ascending asthenospheric diapir centred to the southeast of Zabargad Island as suggested by geophysical data (Styles and Gerdes, 1983).

Acknowledgements

The authors gratefully acknowledge Hannes Brueckner and Jacques Touret for their constructive reviews and Monique Seyler for fruitful discussions. The authors wish to thank Neil Mancktelow for providing the StereoPlot software, Marie-Christine Boiron for Raman analysis and Alain Kohler for MEB investigations. Contribution CRPG number 1225.

References

Agrinier, P., Mével, C., Bosch, D., Javoy, M., 1993. Metasomatic hydrous fluids in amphibole peridotites from Zabargad Island (Red Sea). Earth and Planetary Science Letters 120, 187–205.

Bodnar, R.J., 1994. Synthetic fluid inclusions XII: experimental determination of the liquidus and isochores for a 40 wt.% H_2O–NaCl solution. Geochim. Cosmochim. Acta 49, 1861–1873.

Bodnar, R.J., Vityk, M.O., 1994. Interpretation of microthermometric data for H_2O–NaCl fluid inclusions. In: De Vivo, B., Frezzotti, M.L. (Eds.), Fluid Inclusions in Minerals: Methods and Applications. Short Course, Intenational Mineralogical Association, pp. 117–130.

Bodnar, R.J., Binns, P.R., Hall, D.L., 1989. Synthetic fluid inclusions VI. Quantitative evaluation of the decrepitation behaviour of fluid inclusions in quartz at one atmosphere confining pressure. J. Metamorph. Geol. 7, 229–242.

Bohannon, R.G., 1989. Style of extensional tectonism during rifting, Red Sea and Gulf of Aden. J. Afr. Earth Sci. 8, 589–602.

Bonatti, E., Seyler, M., 1987. Crustal underplating and evolution in the Red Sea rift: uplifted gabbro/gneiss crustal complexes on Zabargad and brothers Islands. J. Geophys. Res. 92, 12803–12821.

Bonatti, E., Hamlyn, P.R., Ottonello, G., 1981. Upper mantle beneath a young oceanic rift: peridotites from the island of Zabargad (Red Sea). Geology 9, 474–479.

Bonatti, E., Clocchiatti, R., Colantoni, P., Gelmini, R., Marinelli, G., Ottonello, G., Santacroce, R., Taviani, M., Abdel-Meguid, A.A., Assaf, H.S., El Tahir, M.A., 1983. Zabargad (St. John) Island: an uplifted fragment of sub-Red Sea lithosphere. J. Geol. Soc. London 140, 677–690.

Bosch, D., 1991. Introduction d'eau de mer dans le diapir mantellique de Zabagad (Mer Rouge) d'après les isotopes du Sr et du Nd. C.R. Acad. Sci. Paris 313, 49–56.

Boudier, F., Nicolas, A., 1991. High temperature hydrothermal alteration of peridotite, Zabargad Island (Red Sea). J. Petrol., Special Lherzolites Issue, pp. 243–253.

Boudier, F., Nicolas, A., Ji, S., Kienast, J.R., Mevel, C., 1988. The gneiss of Zabargad Island: deep crust of a rift. Tectonophysics 150, 209–227.

Boullier, A. 1982. Etude structurale du Précambrien du centre de l'Adrar des Iforas (Mali). Thèse d'Etat, INPL Nancy.

Boullier, A.M., France-Lanord, C., Dubessy, J., Adamy, J., Champenois, M., 1991. Linked fluid and tectonic evolution in the High Himalaya mountains (Nepal). Contrib. Mineral. Petrol. 107, 358–372.

Boullier, A.M., Michot, G., Pêcher, A., Barrès, O., 1989. Diffusion and/or plastic deformation around fluid inclusions in synthetic quartz: new investigations. In: Bridgwater, D. (Ed.), Fluid Movements — Element Transport and the Composition of the Deep Crust. Kluwer, Dordrecht, pp. 345–360.

Bowers, T.S., Helgeson, H.C., 1983. Calculation of the thermodynamics and geochemical consequences of nonideal mixing in the system H_2O–CO_2–NaCl on phase relations in geological systems: equation of state for H_2O–CO_2–NaCl fluids at high pressures and temperatures. Geochim. Cosmochim. Acta 47, 1247–1275.

Brown, P.E., Hagemann, S.G., 1994. MacFlincor: a computer program for fluid inclusion data reduction and manipulation. In: De Vivo, B., Frezzotti, M.L. (Eds.), Fluid Inclusions in

Minerals: Methods and Applications. Short Course, Intenational Mineralogical Association, pp. 231–250.

Brueckner, H.K., Zindler, A., Seyler, M., Bonatti, E., 1988. Zabargad and the isotopic evolution of the sub-Red Sea mantle and crust. Tectonophysics 150, 163–176.

Brueckner, H.K., Elhaddad, M.A., Hamelin, B., Hemming, S., Kröner, A., Reisberg, L., Seyler, M., 1995. A Pan-African origin and uplift for the gneisses and peridotites of Zabargad Island, Red Sea: a Nd, Sr, Pb and Os isotope study. J. Geophys. Res. 100, 22283–22297.

Clocchiatti, R., Massare, D., Jéhanno, C., 1981. Origine hydrothermale des olivines gemmes de l'île de Zabargad (St. Johns) Mer Rouge, par l'étude des inclusions fluides. Bull. Minéral. 104, 354–360.

Coolen, J.J.M.M.M., 1980. Chemical petrology of the Furua granulite complex, southern Tanzania. G.U.A. Pap. Geol. 1 (13), 258.

Dupuy, C., Mével, C., Bodinier, J.L., Savoyant, L., 1991. Zabargad peridotite: evidence for multistage metasomatism during Red Sea rifting. Geology 19, 722–725.

El Ramly, M.F., 1972. A new geological map of the basement rocks in the Eastern and Southwestern deserts of Egypt, scale 1 : 1,000,000. Ann. Geol. Surv. Egypt 11, 1–18.

Féraud, G., Zumbo, V., Sebai, A., Bertrand, H., 1991. $^{40}Ar/^{39}Ar$ age and duration of tholeiitic magmatism related to the early opening of the Red Sea rift. Geophys. Res. Lett. 18, 195–198.

Harley, S.L., 1989. The origins of granulites: a metamorphic perspective. Geol. Mag. 126, 215–247.

Hollister, L.S., 1990. Enrichment of CO_2 in fluid inclusions in quartz by removal of H_2O during crystal–plastic deformation. J. Struct. Geol. 12, 895–901.

Jacobs, G.K., Kerrick, D.M., 1981. Methane: an equation of state with application to the ternary system H_2O–CO_2–CH_4. Geochim. Cosmochim. Acta 19, 607–614.

Ji, S., Mainprice, D., Boudier, F., 1988. Sense of shear in high-temperature movement zones from the fabric asymmetry of plagioclase feldspars. J. Struct. Geol. 10, 73–81.

Kröner, A., Greiling, R., Reischmann, T., Hussein, I.M., Stern, R.J., Dürr, S., Krüger, J., Zimmer, M., 1987. Pan-African crustal evolution in the Nubian segment of northeast Africa. In: Kröner, A. (Ed.), Proterozoic Lithospheric Evolution. Am. Geophys. Union, Geodyn. Ser. 17, 235–257.

Kurat, G., Palme, H., Embey-Isztin, A., Touret, J., Ntaflos, T., Spettel, B., Brandstätter, F., Palme, C., Dreibus, G., Prinz, M., 1993. Petrology and geochemistry of associated vein rocks of zabargad Island, Red Sea, Egypt. Mineral. Petrol. 48, 309–341.

Lancelot, J.R., Bosch, D., 1991. A Pan African age for HP–HT granulite gneisses of Zabargad island: implications for the early stages of the Red Sea rifting. Earth Planet. Sci. Lett. 107, 539–549.

Le Pichon, X., Gaulier, J.M., 1988. The rotation of Arabia and the Levant fault system. Tectonophysics 153, 271–294.

Leroy, J., 1979. Contribution à l'étalonnage de la pression interne des inclusions fluides lors de leur décrépitation. Bull. Minéral. 102, 584–593.

Lespinasse, M., Pêcher, A., 1986. Microfracturing and regional stress field: a study of the preferred orientations of fluid-inclusion planes in a granite from the Massif Central, France. J. Struct. Geol. 8 (2), 169–180.

Marshak, S., Bonatti, E., Brueckner, H., Paulsen, T., 1992. Fracture-zone tectonics at Zabargad Island, Red Sea (Egypt) . Tectonophysics 216, 379–385.

Mezger, K., Essene, E.J., Halliday, A.N., 1992. Closure temperatures of the Sm–Nd system in metamorphic garnets. Earth Planet. Sci. Lett. 113, 397–409.

Munz, I.A., Yardley, B.W.D., Banks, D.A., Wayne, D., 1995. Deep penetration of sedimentary fluids into basement rocks from southern Norway: evidence from hydrocarbon and brine inclusions in quartz veins. Geochim. Cosmochim. Acta 59, 239–254.

Nicolas, A., Poirier, J.P., 1976. Crystalline Plasticity and Solid-State Flow in Metamorphic Rocks. Wiley, London, 444 pp.

Nicolas, A., Boudier, F., Lyberis, N., Montigny, R., Guennoc, P., 1985. L'île de Zabargad (Saint Jean): témoin-clé de l'expansion précoce en Mer Rouge. C.R. Acad. Sci. Paris 301, 1063–1068.

Nicolas, A., Boudier, F., Montigny, R., 1987. Structure of Zabargad Island and early rifting of the Red Sea. J. Geophys. Res. 92, 461–474.

Oberli, F., Ntaflos, Th., Meier, M., Kurat, G., 1987. Emplacement age of the peridotites from Zabargad Island (Red Sea): a zircon U–Pb isotope study. Terra Cognita 7, 334.

Pêcher, A., Boullier, A.M., 1984. Evolution à pression et température élevées d'inclusions fluides dans un quartz synthétique. Bull. Minéral. 107, 139–153.

Percival, J.A., 1989. Granulite terranes and the lower crust of the Superior Province. In: Mereu, R.F., Mueller, S., Fountain, D.M. (Eds.), Properties and Processes of Earth's Lower Crust. Am. Geophys. Union, Geophys. Monogr. 51, 301–310.

Perkins, D.I., Newton, R.C., 1981. Charnockite geobarometers based on coexisting garnet–pyroxene plagioclase–quartz. Nature 293, 144–146.

Ploegsma, M., 1989. Shear zones in the West Uusimaa area, SW Finland. Ph.D. Thesis, Vrije Universiteit Amsterdam, 134 pp.

Ramboz, C., Oudin, E., Thisse, Y., 1988. Geyser-type discharge in Atlantis II Deep, Red Sea: evidence of boiling from fluid inclusions in epigenetic anhydrite. Can. Mineral. 26, 765–786.

Roedder, E., 1984. Fluid Inclusions. Mineralogical Society of America, 646 pp.

Santosh, M., 1986. Carbonic metamorphism of charnockites in the southwestern Indian shield: a fluid inclusion study. Lithos 19, 1–10.

Santosh, M., Jackson, D.H., Harris, N.B.W., Mattey, D.P., 1991. Carbonic fluid inclusions in South Indian granulites: evidence for entrapment during charnockite formation. Contrib. Mineral. Petrol. 108, 318–330.

Schiffries, C.M., 1990. Liquid-absent aqueous fluid inclusions and phase equilibria in the system $CaCl_2$–NaCl–H_2O. Geochim. Cosmochim. Acta 54, 611–619.

Seyler, M., Bonatti, E., 1988. Petrology of a gneiss/amphibolite metamorphic unit from Zabargad Island. Tectonophysics 150, 177–207.

Sibson, R.H., 1990. Faulting and fluid flow. In: Nesbitt, B.E.

(Ed.), Fluids in Tectonically Active Regimes of the Continental Crust. Mineralogical Association of Canada, 18, pp. 93–132.

Sterner, S.M., Bodnar, R.J., 1989. Synthetic fluid inclusions, VII. Re-equilibration of fluid inclusions in quartz during laboratory. Simulated metamorphic burial and uplift. J. Metamorph. Geol. 7, 243–360.

Styles, P., Gerdes, K.D., 1983. St. John's Island (Red Sea): a new geophysical model and implications for the emplacement of ultramafic rocks in fracture zones and at continental margins. Earth Planet. Sci. Lett. 65, 353–368.

Sultan, M., Becker, R., Arvidson, R.E., Shore, P., Stern, R.J., El Alfy, A., Attia, R.I., 1993. New constraints on Red Sea rifting from correlations of Arabian and Nubian Neoproterozoic outcrops. Tectonics 12, 1303–1319.

Tapponnier, P., Brace, W.P., 1976. Stress induced microcracks in Westerly granite . Int. J. Rock Mech. Miner. Sci. 13, 103–112.

Touret, J., 1981. Fluid inclusions in high-grade metamorphic rocks. In: Hollister, L.S., Crawford, M.L. (Eds.), Fluid Inclusions: Applications to Petrology. Mineralogical Association of Canada, 6, pp. 182–208.

Touret, J., 1987. Fluid distribution in the continental lithosphere. In: Kröner, A. (Ed.), Proterozoic Lithospheric Evolution. Am. Geophys. Union, Geodyn. Ser., 17, 27–33.

Tuttle, O.F., 1949. Structural petrology of planes of liquid inclusions. J. Geology 57, 331–356.

Vityk, M., Bodnar, R., 1995. Textural evolution of synthetic fluid inclusions in quartz during reequilibration, with applications to tectonic reconstruction. Contrib. Mineral. Petrol. 121, 309–323.

Wells, P.R.A., 1977. Pyroxene geothermometry in simple and complex system. Contrib. Mineral. Petrol. 62, 129–139.

Wise, D.U., 1964. Microjointing in basement, middle Rocky mountains of Montana and Wyoming. Bull. Geol. Soc. Am. 75, 287–306.